University of Zurich[UZH]

Zurich Open Repository and Archive
University of Zurich
University Library
Strickhofstrasse 39
CH-8057 Zurich
www.zora.uzh.ch

Year: 2018

A MEMS condenser microphone based acoustic receiver for totally implantable cochlear implants

Pfiffner, Flurin ; Prochazka, Lukas ; Dobrev, Ivo ; Dalbert, Adrian ; Sim, Jae Hoon ; Harris, Francesca ; Guignard, Jeremie ; Walraevens, Joris ; Röösli, Christof ; Huber, Alex

Abstract: The goal of the present project is to develop intracochlear acoustic receivers (ICAR's) for measurement of the sound pressure in the inner ear of human temporal bones and in acute large animal experiments. In addition, the ICAR is designed to be used as an implantable microphone for totally implantable cochlear implant (TICI) systems. The presented ICAR concept is based on a commercially available MEMS condenser microphone customized with a protective diaphragm providing sealing properties and optimized sensor head geometry for accessing the tiny fluid-filled cavities of the human inner ear. The first ICAR prototypes (PT I) have been used for numerous intracochlear sound pressure measurements in human and sheep temporal bones. The data thus obtained are in good agreement with the literature. The second ICAR prototype (PT II) was further adapted for surgical insertion in the scala tympani in acute large animal experiments. First experiments have been successfully performed and further revealed that the presented ICAR concept is a suitable receiver technology for TICI systems. Currently, the development of a fully biocompatible ICAR (PT III) is ongoing. This sensor must fulfill all important requirements of a TICI device such as high performance, low power consumption and good system integration.

DOI: https://doi.org/10.1121/1.5035819

Posted at the Zurich Open Repository and Archive, University of Zurich
ZORA URL: https://doi.org/10.5167/uzh-151589
Journal Article
Published Version

Originally published at:
Pfiffner, Flurin; Prochazka, Lukas; Dobrev, Ivo; Dalbert, Adrian; Sim, Jae Hoon; Harris, Francesca; Guignard, Jeremie; Walraevens, Joris; Röösli, Christof; Huber, Alex (2018). A MEMS condenser microphone based acoustic receiver for totally implantable cochlear implants. Journal of the Acoustical Society of America, 143(3):1778.
DOI: https://doi.org/10.1121/1.5035819

A MEMS Condenser Microphone-Based Intracochlear Acoustic Receiver

Flurin Pfiffner*, *Member, IEEE*, Lukas Prochazka, Dominik Péus, Ivo Dobrev, Adrian Dalbert, Jae Hoon Sim, Rahel Kesterke, Joris Walraevens, Francesca Harris, Christof Röösli, Dominik Obrist, and Alexander Huber

Abstract*—*Goal: **Intracochlear sound pressure (ICSP) measurements are limited by the small dimensions of the human inner ear and the requirements imposed by the liquid medium. A robust intracochlear acoustic receiver (ICAR) for repeated use with a simple data acquisition system that provides the required high sensitivity and small dimensions does not yet exist. The work described in this report aims to fill this gap and presents a new microelectromechanical systems (MEMS) condenser microphone (CMIC)-based ICAR concept suitable for ICSP measurements in human temporal bones. *Methods:* The ICAR head consisted of a passive protective diaphragm (PD) sealing the MEMS CMIC against the liquid medium, enabling insertion into the inner ear. The components of the MEMS CMIC-based ICAR were expressed by a lumped element model (LEM) and compared to the performance of successfully fabricated ICARs. *Results:* Good agreement was achieved between the LEM and the measurements with different sizes of the PD. The ICSP measurements in a human cadaver temporal bone yielded data in agreement with the literature. *Conclusion:* Our results confirm that the presented MEMS CMIC-based ICAR is a promising technology for measuring ICSP in human temporal bones in the audible frequency range. *Significance:* A sensor for evaluation of the biomechanical hearing process by quantification of ICSP is presented. The concept has potential as an acoustic receiver in totally implantable cochlear implants.**

***Index Terms*—Acoustic transducer, inner ear sensor, intracochlear sound pressure, Microelectromechanical systems (MEMS) condenser microphone, sound pressure transducer.**

Manuscript received September 18, 2016; revised November 16, 2016; accepted December 13, 2016. Date of publication December 16, 2016; date of current version September 18, 2017. This work was supported by the Baugartenstiftung Zürich, Switzerland, by the Cochlear Technology Centre Belgium, by Cochlear AG, European Headquarters, Switzerland, and the Swiss National Science Foundation under Grant 153396. *Asterisk indicates corresponding author.*

*F. Pfiffner was with the Cochlear AG, European Headquarters, Basel CH-4052, Switzerland. He is now with the University of Zurich, University Hospital Zurich, Department of Otorhinolaryngology, Head and Neck Surgery, Zurich 8091, Switzerland (e-mail: flurin.pfiffner@usz.ch).

L. Prochazka was with the Institute of Fluid Dynamics, Swiss Federal Institute of Technology in Zurich. He is now with the streamwise gmbh.

D. Péus, I. Dobrev, A. Dalbert, J. H. Sim, R. Kesterke, C. Röösli, and A. Huber are with the University of Zurich, University Hospital Zurich, Department of Otorhinolaryngology, Head and Neck Surgery.

J. Walraevens and F. Harris are with the Cochlear Technology Centre.

D. Obrist is with the ARTORG Center, University of Bern.

Digital Object Identifier 10.1109/TBME.2016.2640447

I. Introduction

TRANSMISSION and transformation of airborne sound through the outer and middle ear (ME) into sound pressure in the inner ear (i.e., cochlea) fluid is a fundamental biomechanical process of hearing. Sound measurements along this pathway help us to determine sound transmission in normal hearing and conductive hearing disorders. The findings from these experimental approaches and the deduced theoretical models contribute to the understanding of hearing and have led to improved hearing rehabilitation with surgical interventions and implantable hearing devices [1]–[4]. Further investigations of the biomechanical hearing process are important for optimization of future hearing rehabilitation methods.

Quantification of intracochlear sound pressure (ICSP) [5] is an objective measurement for evaluation of the complete biomechanical hearing process from the outer to the inner ear. Methods to measure ICSP are mainly limited by the small dimensions of the fluid-filled cochlea and the spatially constrained surgical access into the cochlea. The sensing component of the applied intracochlear acoustic receiver (ICAR) has to be smaller than the basal part of the scala tympani (ST), with an average cross-sectional height of 1.25 mm and average width of 1.66 mm [6], [7]. Besides the dimensional constraints, an ICAR working in a liquid medium must provide high sensitivity and a low noise floor with a sufficient signal-to-noise ratio (SNR). An SNR of 30 dB or better is targeted to determine the inner ear pressure in human temporal bones experimentally. Stimulation levels of up to 100 dB sound pressure level (SPL) can be applied in the ear canal (EC); therefore, an ICAR with a maximum equivalent input noise (EIN) of 70 dB SPL is needed. The ICAR is designed to cover the frequency range of 250 to 8000 Hz, which is important for speech understanding.

An ICAR fulfilling these requirements with a robust design suitable for repeated use and compatibility with a simple data acquisition system is not yet available. This paper presents a new ICAR for ICSP measurements aimed at filling that gap.

In addition, we aimed for an ICAR concept that would also be suitable for use in new future applications. Such applications include chronic *in vivo* animal experiments and potential use as an implantable microphone for totally implantable hearing devices (e.g., cochlear implants [8]). This imposes additional requirements on the ICAR sensor concept, such as biocompatibility,

0018-9294 © 2016 IEEE. Personal use is permitted, but republication/redistribution requires IEEE permission.
See http://www.ieee.org/publications_standards/publications/rights/index.html for more information.

low power consumption, and a compact design for an implantable sensor read-out system.

In this publication, we: 1) present a sensor concept fulfilling requirements for ICSP measurements in human temporal bones; 2) introduce a sensor lumped element model (LEM); 3) present a fabricated sensor based on the LEM; 4) validate the sensor's LEM experimentally; and 5) apply the sensor for the quantification of the ICSP in human temporal bones experimentally.

II. Sensor Design

In acoustic sensing, sound energy is measured by capacitive, piezoresistive, electromagnetic, optical, or piezoelectric transduction principles. With the exception of the piezoelectric sensors, all of these sensing methods require a flexible diaphragm as a sound receiving element to capture the sound induced pressure fluctuations of the fluid medium. In previous studies, ICSP in mammals has been measured with: piezoelectric sensors [9] in cats; piezoresistive sensors [10]–[12] in guinea pigs; and fiber-optic-based sensors [5], [13]–[16] in gerbils. In human cadaver heads, ICSP has been quantified with strain gauges [17] and fiber-optic-based sound pressure sensors [18], [19]. However, the broader application of existing ICSP measurement methods is limited by laborious sensor preparation, sensor sensitivity changes related to biomaterial deposits on the sensing elements, complexity of the experimental ICSP measurement setup, and low sensor SNR.

Fiber-optic-based ICARs [14], [15] have a high SNR but suffer from high power consumption, complex signal read-out hardware with a large form factor, and failure to meet the requirements for integration into existing implantable medical devices. In comparison, ICARs, based on capacitive transduction of an electric field related to the displacement of an acoustically excited membrane, have the highest sensitivity compared to ICARs with piezoresistive, electromagnetic, or piezoelectric transduction mechanisms, combined with low power consumption [20], [21]. Therefore, we chose capacitive transduction as the most promising principle for use in our ICAR concept.

In the last decade, micro-electro-mechanical system (MEMS) technology has rapidly progressed, driven largely by the market for consumer electronics [22]. Commercially available MEMS condenser microphones (CMIC) are increasingly replacing existing microphone technology (electret condenser microphones) for hearing aid devices [23], [24]. Further, it is anticipated that these development efforts will continue and will lead to even better performing MEMS CMICs with smaller size, higher sensitivity, lower noise floor, lower power consumption, and suitability for mass-production applications due to their compatibility with reflow soldering [25]–[28].

Analog MEMS CMICs consist of a transducer (capacitor) and an application-specific integrated circuit unit including a preamplifier, which reduces the high output impedance of the capacitor to a value suitable for an audio signal chain. Both components are closely packed onto a printed circuit board and are shielded acoustically and electrically by a metallic cap. The capacitor consists of a flexible diaphragm, as the sound

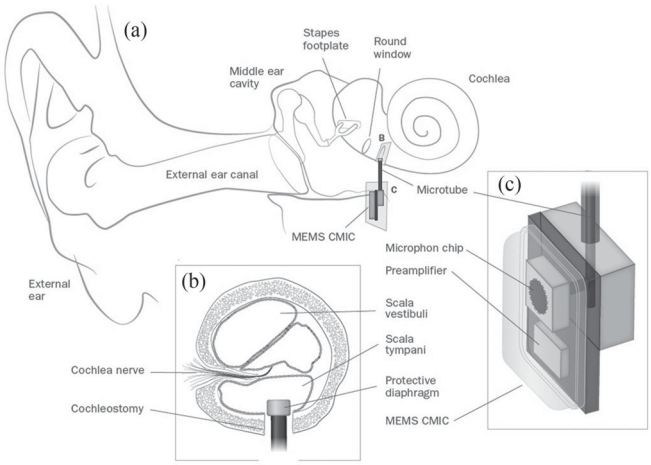

Fig. 1. Anatomical structures of the human ear and MEMS CMIC ICAR location (not to scale). (b) Cross section of basal turn of cochlea and location of the sensor head with PD that picks up inner ear pressure fluctuations. (c) Schematic drawing of the MEMS CMIC-based customized ICAR (Fig. 1 is used with permission from S. Steinbacher, SIVIC, University of Zurich).

pressure sensing element, with a typical area of less than 1 mm^2, a thickness of less than 1 μm, and of a rigid plate, called the back plate, oriented parallel to the diaphragm, with less than 10-μm separation [28]. Current state-of-the-art MEMS CMICs, optimized for use in hearing aid devices, are compact (<12 mm^3), have an EIN below 30 dBA SPL, a sensitivity larger than -40 dB re 1 V/Pa, and a power consumption below 40 μW [29].

These MEMS CMICs are designed for sensing in air (or other gasses) and cannot operate in a liquid environment, mainly because of lacking electrical insulation and nonhermetic diaphragm design, which includes vent holes required to equalize the static pressure between ambient pressure and the sensor's back pressure. In our application, the cochlea fluid would enter through the diaphragm vent holes and degrade the sensor's performance or damage the integrated circuit unless prevented otherwise.

Therefore, our ICAR concept includes an additional passive protective diaphragm (PD) sealing the MEMS CMIC against the liquid working medium on the receiving side. Vibrations of the PD induced by ICSP are transferred to the diaphragm of the MEMS CMIC by pressure fluctuations in the air-filled volume of a connecting microtube between the two deflecting elements. In addition, the PD forms a sensor head that is designed to be sufficiently small to satisfy the size requirements for ICSP measurements.

The MEMS CMIC itself is too large to fit inside the cochlea [see Fig. 1(a)] and is therefore situated in the surgical access cavity to the inner ear. A microtube of several millimeters in length interconnects the PD and the MEMS CMIC (see Fig. 1(b) and 1(c). The PD reduces the receiving sensitivity due to its mechanical compliance and the compliance of the pressurized cavity between the PD and the sensing (i.e., MEMS microphone) diaphragm. The loss in sensitivity is reduced by choosing an optimal PD material, geometry and dimensions, and by minimizing the volume between the two diaphragms.

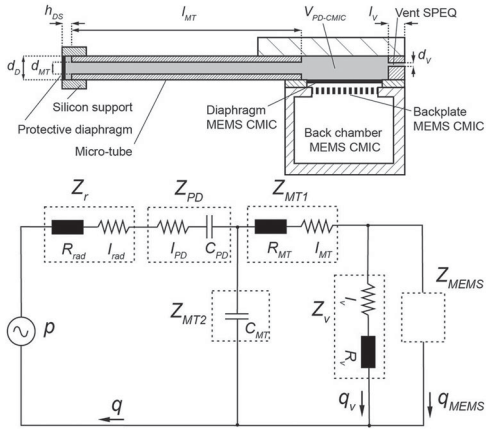

Fig. 2. Schematic diagram of MEMS CMIC-based customized ICAR (top). Equivalent LEM (bottom) including the acoustic impedance of: Z_r, the interaction between surrounding fluid and PD; Z_{PD}, the protective diaphragm; Z_{MT1} and Z_{MT2}, the micro-tube between PD and MEMS CMIC; Z_v, the vent for SPEQ; and Z_{MEMS}, the MEMS CMIC.

Static pressure differences between the internal pressure of the ICAR and ambient pressure create a quasi-static pressure difference across the PD, reducing the acoustic pressure sensitivity of the sensor. A static pressure equalization (SPEQ) system between the ambient pressure and the internal pressure of the ICAR structure is required to minimize this effect. This can be achieved with a vent (acoustic throttle) connecting the internal volume of the ICAR structure to ambient air.

III. Methods

A. Sensor-Lumped Element Models

A theoretical model was used to predict the sensitivity performance of the ICAR concept and to confirm the fulfilment of the sensitivity and dimensional requirements. An electroacoustic sensor such as the MEMS CMIC can be modeled by equivalent circuits composed of lumped elements. Acoustic, mechanical, and electrical elements [see Fig. 2(a)] of a MEMS CMIC, such as the diaphragm, back plate, back cavity, and electrical capacity were represented by acoustic impedances with equivalent mass, stiffness and/or damping properties [30]–[33]. The relevant dimensions of the individual microphone elements, including the microtube size, had to be much smaller than the wavelength of the acoustic wave for such representations [34]. Assuming that the length of the microtube connecting the PD and the MEMS CMIC satisfied this requirement, the transfer function of the ICAR could be approximated using an adapted LEM of a CMIC. A drawing of such an equivalent circuit is shown in Fig. 2.

The MEMS CMIC represented by the acoustic impedance Z_{MEMS} was described using standard LEMs reported in the literature without consideration of effects due to the inlet port and the interaction with the surrounding fluid [31], [35]. The PD was modeled as a moving piston without taking into account the curvature of the deflected clamped plate. The piston was described as a mechanical spring C_{PD} with inertia I_{PD}.

TABLE I
Input Parameters of the ICAR LEM Including CMIC

Part	Parameter	Symbol	Value	Unit
MEMS CMIC				
Diaphragm:	Area	A_d	$0.35^2\pi$	mm^2
	Thickness	t_d	0.5	μm
Diaphragm	Young's modulus	E_d	130	GPa
material: Single	Poisson ratio	ν_d	0.3	
crystal silicon	Density	ρ_d	2330	kg/m^3
Backplate (BP):	Radius	R_{BP}	0.35	mm
	Thickness	T_{BP}	15	μm
Venting holes in	Diameter	d_{v-BP}	15	μm
BP:	Surface fraction	Π	0.35	
Air gap between diaphragm and back plate	Distance	d_g	4	μm
Vent channel for SPEQ	Diameter	d_{vs}	36	μm
	Length	l_{vs}	50	μm
Back cavitiy	Volume	V_c	3.75	mm^3
	Bias voltage	V_{bias}	1	V
Inlet port	Diameter	d_{in}	0.6	mm
	Length	l_{in}	1	mm
ICAR with PD				
PD	Radius	r_{PD}	0.15–0.3	mm
	Thickness	t_{PD}	1	μm
	Area	A_{PD}	0.07–0.28	mm^2
	Apparent Mass (in vacuum)	m_{PD}	(2)	
PD material:	Young's modulus	E_{PD}	8.5	GPa
Polyimide	Poisson ratio	ν	0.2	
PI2611 [36]	Density of the PD	ρ_{PD}	1400	kg/m^3
	Residual stress in PD		2	MPa
PD support structure	Height	h_{DS}	0.38	mm
Microtube	Radius	r_{MT}	0.075	mm
	Length	l_{MT}	5	mm
	Apparent Mass	m_{MT}	eq. 5	
Volume between	Volume	$V_{\mathrm{PD-CMIC}}$	0.3	mm^3
PD and MEMS	Dynamic viscosity	μ_{air}	1.98×10^{-5}	Pa s
CMIC diaphragm	Density	ρ_{air}	1.2	kg/m^3
Vent channel for	Radius	r_v	12.5	μm
SPEQ	Apparent mass	m_v	(7)	
	Length	l_v	1.4	mm

Mechanical energy losses within the diaphragm material were neglected. The interaction between PD and surrounding fluid created dissipation R_{rad} caused by radiation of acoustic waves into the far field. It also included a reactive part I_{rad} that was regarded as the moving fluid mass adjacent to the PD (mass loading). The microtube interconnecting the PD and sensing diaphragm influenced the inertia, damping, and acoustic stiffness of the system. Therefore, it was described by a dissipative R_{MT} and inertial impedance I_{MT}, which were connected in series with the lumped element Z_{PD}, the fluid adjacent to the PD Z_r, and the unsealed microphone Z_{MEMS} [see Fig. 2(b)]. The lumped element describing the acoustic stiffness of the microtube Z_{MT2} was connected in parallel to Z_{MT1} and Z_{MEMS}. The vent for SPEQ was regarded as an acoustic throttle pressurizing the interior of the sensor structure at the interface between the microtube and MEMS CMIC. It was modeled as a lumped element Z_V, a serial connection of a dissipative element R_V, and an inertial element I_V, which short circuited the MEMS CMIC for sound pressures below a certain low cutoff frequency. The values of all input parameters characterizing the LEM of the ICAR are summarized in Table I. All lumped elements

representing the ICAR were described by semiempirical analytical solutions, as listed in Table II.

The open-circuit voltage sensitivity S_v of the ICAR was calculated using (8) in Table I. The response of the MEMS CMIC's diaphragm to incoming pressure fluctuations was expressed as velocity u_{MEMS}, which was determined from the electrical circuitry by solving for the volume flow through the CMIC, $q_{\mathrm{MEMS}} = u_{\mathrm{MEMS}} \times A_d$. It is the sum of the volume flow through the main energy path of the CMIC, represented by the diaphragm, the back plate, and the volume flow through their bypass (acoustic throttle) required for SPEQ.

First, the frequency response of the unsealed MEMS CMIC was calculated using the LEM and expressed as the open-circuit sensitivity S_v shown in Fig. 3 (dotted black line). The unsealed case was calculated for fine adjustment of the LEM representing the MEMS CMIC by matching reference data from the device datasheet [29] (cf., blue solid line in Fig. 3). Fine tuning of the LEM was necessary due to lack of precise information concerning dimensions and electrical properties of the MEMS CMIC.

Second, the sensitivity of the ICAR, including the additional sealing parts was calculated on the basis of the LEM. As the PD area significantly impacted the sensitivity, several PD sizes were chosen in order to validate the LEM. As the PD diameter was limited by the anatomical dimensions of the cochlea, PD diameters of 0.3, 0.38, 0.5, and 0.6 mm were used. Similar to the performance of the unsealed CMIC, the ICAR showed a flat frequency response well below the resonance frequency. Within that frequency range, the sensor's performance was solely governed by the mechanical compliance of the system. The resonance frequency of ICAR, which defines the upper limit of the usable measurement bandwidth, was lower than for the unsealed device. It also decreased for larger PD diameters. In contrast to the MEMS CMIC operating in air, where the resonance was governed by the interaction between the acoustic inlet port and the acoustic compliance of the sensor (cf., Helmholtz resonator), the resonance of the ICAR was mainly influenced by the high inertia of a fluid-loaded PD. The lower frequency limit of the ICAR was defined by the high pass characteristics of the acoustic throttle (vent) used for the SPEQ. It was situated well below 250 Hz. The ICAR with 0.6 mm PD showed 20 dB lower sensitivity and a bandwidth that was three times smaller compared to the unsealed CMIC. To meet the sensing performance requirements stated in Section I, the PD diameter had to be between 0.3 and 0.38 mm.

B. Sensor Design and Fabrication

Several MEMS CMIC-based ICARs were fabricated on the basis of the LEM results. Fig. 4 illustrates an enlarged drawing of the ICAR design, consisting of the sound receptor, the MEMS CMIC, the amplifier unit, the tube for SPEQ, and the connector interface. The sound receptor was a 1-μm-thick polyimide diaphragm (PI 2610, HD MicroSystems GmbH, Germany) supported by a thin-walled cylindrical structure made of single crystal silicon. The outer and inner diaphragm diameters were 0.5 and 0.38 mm, respectively. Further sound receptor sizes

TABLE II
LEM REPRESENTING THE ICAR BY SEMIEMPIRICAL ANALYTICAL SOLUTIONS

Symbol	Parameter	Equation
Z_r	Acoustic radiation impedance [kg/s/m^4] interaction between cochlea fluid and PD [34]	
R_r	Radiation resistance [kg/s] density surrounding fluid	$R_r = \frac{\pi}{4}\rho_S\, ck^2 {r_{\mathrm{PD}}}^4$
ρ_S	[kg/m^3]	$X_r = 1.9\omega\rho_S {r_{\mathrm{PD}}}^3$
k	Angular wave number [rad/m]	$Z_r = \frac{1}{A_{\mathrm{PD}}^2}(R_r + \mathrm{i}X_r)$ (1)
Xr	Acoustic radiation mass [kg/s]	
ω	Angular frequency [rad/s]	
Z_{PD}	Acoustic impedance [kg/s/m^4] of the PD	
C_{PD}	Mechanical compliance of the PD [m/N]	$C_{\mathrm{PD}} = \frac{1}{A_{\mathrm{PD}}}S_m = \frac{1}{A_{\mathrm{PD}}}\frac{dw}{dp}\vert_{w=0}$
		$m_{\mathrm{PD}} = \frac{1}{C_{\mathrm{PD}}{\omega_{r0}}^2}$
ω_{r0}	Natural angular frequency of a flat circular diaphragm [rad/s]	$Z_{\mathrm{PD}} = \frac{1}{A_{\mathrm{PD}}^2}\left(\mathrm{i}\omega m_{\mathrm{PD}} + \frac{1}{\mathrm{i}\omega C_{\mathrm{PD}}}\right)$ (2)
S_m	Mechanical sensitivity of the PD [m^3/N]	$\frac{p{r_{\mathrm{PD}}}^4}{E_{\mathrm{PD}}{t_{\mathrm{PD}}}^4} =$
	Pressure-deflection relation for a flat, clamped, circular diaphragm with residual stress and for large deflections [37]	$\left(\frac{16}{3(1-^2)} + \frac{4\sigma {r_{\mathrm{PD}}}^2}{E_{\mathrm{PD}}{t_{\mathrm{PD}}}^2}\right)\left(\frac{w}{t_{\mathrm{PD}}}\right) + \frac{2.83}{1-^2}\left(\frac{w^3}{t_{\mathrm{PD}}^3}\right)$ (3)
p	Pressure load [Pa]	$k_t = \frac{r_{\mathrm{PD}}}{t_{\mathrm{PD}}}\sqrt{\frac{12(1-^2)\sigma}{E_{\mathrm{PD}}}}$
w	Center diaphragm deflection [m]	
k_t	Tension parameter [38]	${\omega_{r0}}^2 = \frac{D}{\rho_{\mathrm{PD}}t_{\mathrm{PD}}r_{\mathrm{PD}}^4}\varepsilon^2[\varepsilon^2 + k_t^2]$ (4)
ε	Characteristic variable (adapted from Fig. 2 in [38])	
Z_{MT1}, Z_{MT2}	Acoustic impedance [kg/s/m^4] of intermediate volume between PD and CMIC $\mathrm{V_{PD-CMIC}}$ (cf., gray shaded area Fig 2(a) [34]	$m_{\mathrm{MT}} = \frac{4}{3}\frac{\rho_{\mathrm{air}M\,T}\, l_{\mathrm{MT}}}{\pi {r_{\mathrm{MT}}^4}^2 A_{\mathrm{MT}}}$
R_{MT}	Acoustic resistance of MT [kg/s/m^4]	$R_{\mathrm{MT}} = 8\frac{\mu_{\mathrm{air}}l_{\mathrm{MT}}}{\pi r_{\mathrm{MT}}^4}$
		$Z_{\mathrm{MT1}} = R_{\mathrm{MT}} + \mathrm{i}\omega m_{\mathrm{MT}}$ (5)
$C_{\mathrm{PD-CMIC}}$	Acoustic compliance of the volume $\mathrm{V_{PD-CMIC}}$	$C_{\mathrm{PD-CMIC}} = \frac{V_{\mathrm{PD-CMIC}}}{c^2\rho_{\mathrm{air}}}$
		$Z_{\mathrm{MT2}} = 1/i\omega C_{\mathrm{PD-CMIC}}$ (6)
Z_v	Acoustic impedance [kg/s/m^4] of the vent for SPEQ [34]	
		$m_v = \frac{4}{3}\frac{\rho_{\mathrm{air}}(l_v + 2\times 0.85\times r_v)}{A_v}$
Rv	Acoustic resistance of vent for SPEQ	$R_v = 8\frac{\mu_{\mathrm{air}}l_v}{\pi r_v^4}$
		$Z_v = R_v + i\omega m_v$ (7)
Z_{MEMS}	Acoustic impedance of the MEMS CMIC adapted from [31]	
S_v	Open-circuit voltage sensitivity [V/Pa]	
V_o	Open-curcuit voltage at the microphones's electrical output	
u_{MEMS}	Velocity of the MEMS CMIC's diaphragm	
p_o	incoming sound pressure	$S_v = \left\vert\frac{V_o}{p}\right\vert = \left\vert\frac{V_b\, u_{\mathrm{MEMS}}}{i\omega d_g}\right\vert$ (8)

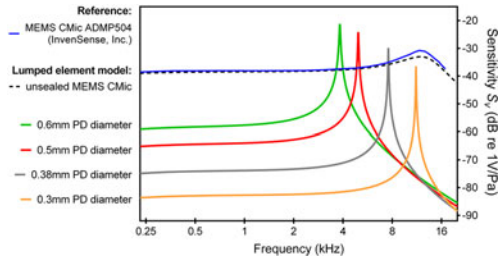

Fig. 3. Frequency response of the ICAR expressed as open-circuit voltage sensitivity and calculated by the LEM (8). Four different PD diameters are compared to the unsealed MEMS CMIC (blue line) and reference data from the ADMP 504 MEMS CMIC [29] (black dotted line).

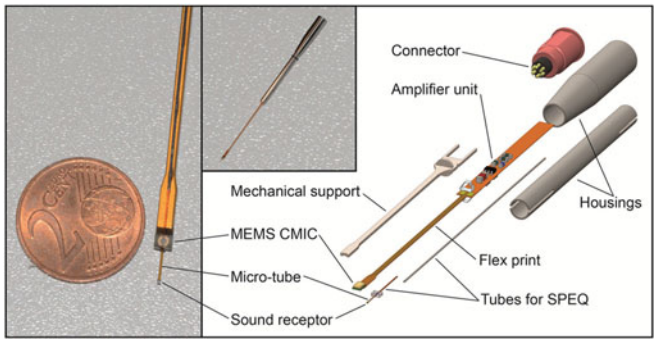

Fig. 4. Photographs of a zoomed-in view of the sensor head and completely assembled ICAR (left and middle). Enlarged assembly drawing with components (right).

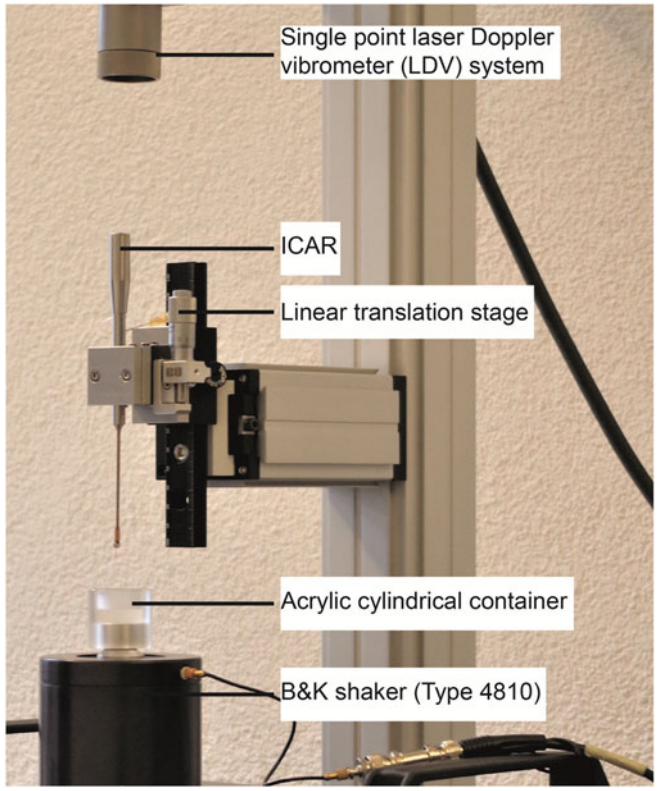

Fig. 5. Photographs of the ICAR calibration setup.

with PD diameters 0.3, 0.5, and 0.6 mm were also available for testing. The glass microtube, interconnecting the sound receptor and the MEMS microphone, had an inner diameter of 150 μm and a length of 5 mm. A commercially available MEMS CMIC was used (ADMP504 MEMS CMIC from Analog Devices Inc., US). A flexible printed circuit electrically interconnected the MEMS microphone and the operational amplifier unit (type ADA4004, Analog Devices Inc., USA). A laser cut beam structure of stainless steel provided sufficient mechanical support for the sensor probe. For the first 5 mm, the SPEQ system consisted of a fused silica tube with an internal diameter of 25 μm (acoustic throttle). The adjacent SPEQ tube led the pressure port into the amplifier housing. SPEQ tube and amplifier housing were made of stainless steel.

C. Sensor Calibration

The frequency response of the ICARs was determined to validate the LEM and to monitor changes of the ICAR's sensitivity prior to and after the experiments. The calibration technique was based on a vibrating water column that has been used for similar applications [14], [39]. This technique is based on the pressure variation p for a sensor head with an immersion depth h due to the harmonically varying hydrostatic pressure and the inertia of the water column above the sensor head. It is given by

$$p = \rho g x + \rho h \ddot{x} = \rho x_0 \left(g + \omega^2 h\right) \ . \qquad (1)$$

The displacement of fluid from the initial position was depicted as x and the amplitude as x_0 with ρ the fluid density and ω the angular frequency. This calibration method required that the ICAR's head be much smaller than the depth of immersion in order to minimize boundary effects [40]. Thus, the dimensions of the sensor head defined the size of the water column container and the upper limit of the usable bandwidth of the calibration system. The corner frequency was given either by the mechanical resonance frequency of the support structure or the first acoustic vibration mode of the water column. For the present setup, a shaker (Type 4810, Brüel & Kjær Sound & Vibration Measurement A/S, Denmark) was used in combination with an acrylic cylindrical container with outer diameter and height of 30 mm (see Fig. 5). The container held a water column with a diameter of 15 mm and a height of 12 mm. The ICAR was attached to a linear translation stage with a positioning accuracy of 10 μm to adjust the immersion depth. A single point laser Doppler vibrometer (LDV) system (CLV-2534-3, Polytec GmbH, Germany) was used as a reference accelerometer to monitor vibrations orthogonally to the rim of the container. The vibration exciter was driven by an audio analyzer system (APx585, Audio Precision Inc., USA) via a power amplifier (type RMX 850, QSC Audio Products LLC, USA). A custom-built software application (LabVIEW, Version 2013 SR1, NI, US) was used for simultaneous data acquisition of the velocity measured by the LDV system and the pressure from the ICAR.

The driving signal of the vibration exciter at 1 kHz was determined such that it induced a signal of 94 dB SPL for an

immersion depth of 2 mm in the water column. The stimulation signal was a stepped frequency sweep with 40 frequency points logarithmically distributed over the frequency range between 200 Hz and 20 kHz. The equivalent excitation SPL and corresponding ICAR frequency response was determined from the acceleration of the water container based on the LDV signal and (9).

D. Sensor Experiments in Human Temporal Bones

Experiments in human temporal bones were approved by the local ethics committee (KEK-ZH-Nr. 2014-0544). Preparation of the human temporal bone for ICSP measurements followed a standard surgical approach [41], [42]. Prior to drilling access to the inner ear, a standard conformity test of the ME was performed by quantifying the ME transfer function and comparing it to the ASTM practice ME standards [3], [43]. The cochlear access (cochleostomy) to the scala tympani (ST, cf., Fig. 1) was drilled approximately 2.5 mm beside the round window with a diamond burr of 0.7 mm diameter under water to prevent entry of air into the cochlea.

A loudspeaker (ER-2, Etymotic Research, USA) and a reference microphone (ER-7C, Etymotic Research, USA) were placed into the artificial EC and acoustically sealed using a foam insert as done in earlier experiments [41], [42]. Acoustic excitation signals were generated by an audio analyzer (APx585 Audio Analyser, Audio Precision Inc., USA) and amplified by an audio amplifier (RMX 850, QSC Audio Products, USA). A stepped frequency sweep with 25 frequency points, logarithmically distributed over the frequency range of 250–8000 Hz, was used as acoustic stimuli. Two analog input channels (APx585 Audio Analyzer, Audio Precision Inc., USA) recorded the ICAR signal and the artificial EC sound pressure from the reference microphone. The raw data were postprocessed by a bandpass filter based on a digital third-order Butterworth filter. Averaging over five subsequent measurements was performed for each frequency of the stepped frequency sweep of the acoustic stimulation in order to reduce the noise floor of the measurements. Data postprocessing and illustration were done using MATLAB (MathWorks Inc., Natick, MA, USA) and GraphPad Prism V5.04 (GraphPad Software Inc., USA), respectively.

To control insertion location, depth and orientation angle of the ICAR's sensor head into the cochlea, a custom-built micromanipulator with seven degrees of freedom was used. The ICAR was positioned on the micromanipulator and navigated into the ST using a surgical microscope and three cameras for visual feedback. Three successive fabricated ICARs were used. After the last experiment, the ICAR was replaced with a CT marker inserted through the cochleostomy. The CT marker was glued in place and the subsequent microcomputed tomography (SKYSCAN 1176, Bruker Corp., US) and reconstruction (Amira version 6.0, Visualization Sciences Group, France) of the temporal bone quantified the position of the marker in order to confirm the measurement location in the ST.

After the experiments in human temporal bones, the ICAR's frequency response was reverified in order to quantify possible sensitivity changes during the experiments. The sensitivity differences between pre- and postexperiments were less than 3 dB over the whole frequency range for all ICARs. Additionally, visual inspection of the ICAR with a surgical microscope confirmed the PDs were intact and free of contamination.

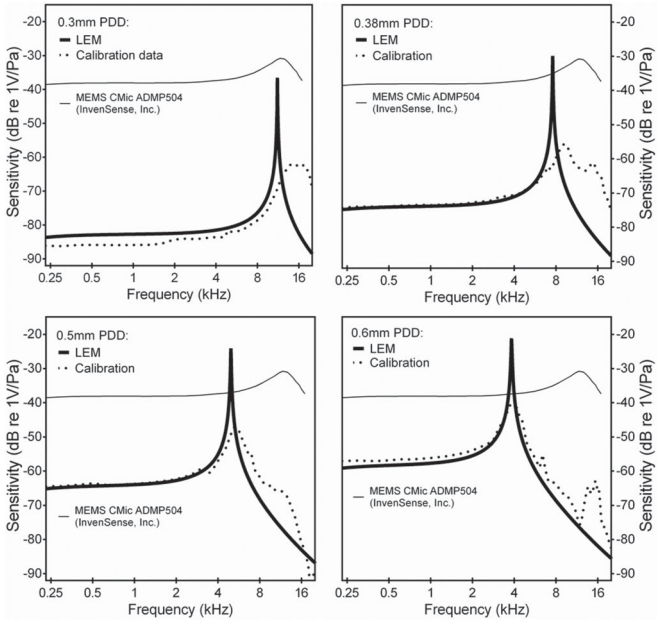

Fig. 6. LEM and calibration measurements for different sizes of the PD diameter. Thick lines represent the LEM, dotted lines the calibration measurement, and thin lines reference data from the ADMP 504 MEMS CMIC [29].

IV. Results

A. Sensor Calibration and LEM Validation

Fine adjustment of the various LEM input parameters was performed to the LEM of the unsealed MEMS CMIC in order to achieve a satisfactory match with reference data. The model parameters representing the dimensions of the sealed MEMS CMIC configurations are mostly well known and did not require fine tuning. However, residual stress within the polyimide PD had a strong influence on the compliance of the PD [cf., (3)], and was dependent on the fabrication process and the supporting material. Furthermore, residual stress was difficult to measure on a small structure such as the sound receptor. We therefore decided to choose a stress level of 2 MPa, as stated in the datasheet of the polyimide diaphragm [36]. Based on that stress level, good agreement between the LEM and the measurement was achieved for all sizes of the PD (cf., Fig. 6). Discrepancy in the flat frequency response range was less than 3 dB, which was within the measurement uncertainty of the ICAR calibration procedure. Larger deviations occurred near the resonance operation range, presumably related to the imprecision in resonance frequency determination using simple semiempirical formulas.

B. ICSP Measurements

Several experiments were performed to measure the ICSP in human temporal bones. Sound pressure measurements in the EC and in the cochlea (ICSP) are shown in Fig. 7. The EC acoustic

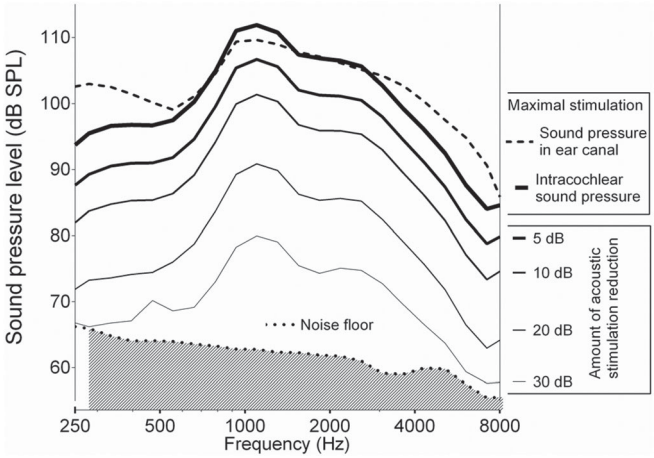

Fig. 7. Acoustic stimulation level in the EC at maximum stimulation (dashed line) recorded by the reference microphone and recorded ICAR signal at maximal stimulation (thick solid line) and with attenuated acoustic stimulation levels (solid lines). The ICAR noise floor is represented by the hashed area below the dotted line.

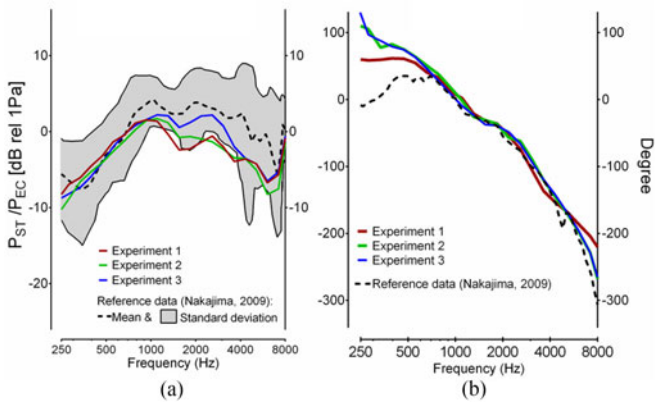

Fig. 8. Left: Intracochlear gain in the ST measured in three experiments (red, green, and blue lines) normalized to the EC SPL in comparison to reference data from [19] (mean as black dashed line, and standard deviation as with grey shaded area). Right: Phase shift between acoustic stimulation in the EC and ICSP in the ST for the same three measurements (red, green, and blue lines) in comparison to reference data from [19] (mean as black dashed line). (a) Gain scala tympani. (b) Phase.

pressure at 110-dB SPL showed frequency dependence in the range of 250 and 8000 Hz with maxima in the mid-frequencies from 0.7–3 kHz (Fig. 7, dashed line). The corresponding ICSP in the ST is shown for different stimulation levels represented by solid lines in Fig. 7. The ICAR was in linear operation range at these stimulation levels, and the pressure gain P_{ST}/P_{EC} in the ST remained constant. The noise floor (Fig. 7, black hashed area) was reached at a reduction in stimulation level of -30 dB at 250 Hz.

To verify repeatability, three fabricated ICARs, equipped with a sound receptor membrane of 0.38 mm diameter, were used sequentially to measure the ICSP in the same temporal bone preparation. The time between the experiments was approximately 30 min. The magnitude and phase of the transfer functions between the EC pressures and the ICSP in the ST, based on measurements with these three ICARs, at a maximum stimulation level of 110 dB SPL are shown in Fig. 8. There was a maximal deviation of 3.5 dB between 1.5 to 3 kHz across the three ICARs, indicating good repeatability. These differences may have been partially related to time dependent changes of the temporal bone preparation [41] and to the discrepancies of a maximum of ± 3 dB between the pre- and postexperimental calibrations.

Nakajima *et al.* [19] presented inner ear pressure measurements in the ST of six human temporal bones using miniature fiber-optic-based sound pressure sensors [14], [15] (cf., Fig. 8). Our measurements were within their reported range for most frequencies. They were somewhat below the mean of the reference data at frequencies above 700 Hz. This is in agreement with data for the ME transfer function of the investigated temporal bone, which also indicated a lower than average ASTM standard response [3], [43] at higher frequencies and consequently lower cochlear input. The corresponding phase of the transfer function is shown in Fig. 8. The phase decreased by approximately 100° per octave above 2 kHz, which is in accordance with reference data from [19].

V. Conclusion

A MEMS CMIC-based ICAR concept was developed to fulfill the major requirements for ICSP measurements in human cadaver temporal bones. The behavior of the sensor was expressed by a LEM and compared to the performance of successfully fabricated MEMS CMIC-based ICARs. A satisfactory agreement between theoretical model and experimental results was achieved. Validation tests in a human cadaver temporal bone at high stimulation levels ($>$85 dB SPL) yielded data in agreement with the literature. We conclude that the presented ICAR concept is a useful sensor with a robust design for measurements of ICSP that could be applied in repeated measurements without marked sensitivity changes.

A future aim is to perform sound pressure measurements in the ST at different locations (mainly farther away from the round window) to gain a better understanding of the hydrodynamics in the human cochlea.

A further optimized MEMS CMIC-based ICAR design may be suitable for use in *in vivo* animal experiments and as an implantable microphone for totally implantable cochlear implants. Compared to other existing ICAR technologies, such as fiber optic-based sound pressure sensors, requirements of biocompatibility, low power consumption, and a compact and implantable sensor read-out system could be fulfilled by the present ICAR concept. The need for higher sensitivity in cochlear implants may be fulfilled with a sensor head that consists of several sound receiving PDs instead of the single PD design. An expanded LEM, accounting for this more complex sensor head design, could be used for predicting the sensitivity and frequency bandwidth, and for defining the dimensional criteria.

Overall, our results confirm that the presented MEMS CMIC-based ICAR is a promising technology to measure the ICSP in human temporal bones in the audible frequency range.

References

[1] R. Aibara *et al.*, "Human middle-ear sound transfer function and cochlear input impedance," *Hearing Res.*, vol. 152, no. 1–2, pp. 100–109, Feb. 2001.

[2] A. M. Huber *et al.*, "The effects of complex stapes motion on the response of the cochlea," *Otol Neurotol.*, vol. 29, no. 8, pp. 1187–92, Dec. 2008.

[3] J. J. Rosowski *et al.*, "Testing a method for quantifying the output of implantable middle ear hearing devices," *Audiol. Neurootol.*, vol. 12, no. 4, pp. 265–76, 2007.

[4] J. H. Sim *et al.*, "Complex stapes motions in human ears," *J. Assoc. Res. Otolaryngol.*, vol. 11, no. 3, pp. 329–341, Sep. 2010.

[5] E. S. Olson, "Direct measurement of intra-cochlear pressure waves," *Nature*, vol. 402, no. 6761, pp. 526–529, Dec. 1999.

[6] M. Zrunek *et al.*, "Dimensions of the scala tympani in relation to the diameters of multichannel electrodes," *Archives Otorhinolaryngol.*, vol. 229, no. 3/4, pp. 159–65, 1980.

[7] J. Zwislocki-Mościcki, "Theorie der Schneckenmechanik," Universitätsklinik für Ohren-, Nasen und Halskrankheiten Basel, ETH Zürich, Zurich, Switzerland, 1948.

[8] Cochlear implant electrode array including receptor and sensor, by J. Walraevens *et al.*, (2013, Nov. 7). Patent WO2015068136. [Online]. Available: http://www.wipo.int

[9] V. Nedzelnitsky, "Sound pressures in the basal turn of the cat cochlea," *J. Acoust Soc. Amer.*, vol. 68, no. 6, pp. 1676–89, Dec. 1980.

[10] P. Avan *et al.*, "Direct evidence of cubic difference tone propagation by intracochlear acoustic pressure measurements in the guinea-pig," *Eur. J. Neurosci.*, vol. 10, no. 5, pp. 1764–1770, 1998.

[11] A. Dancer and R. Franke, "Intracochlear sound pressure measurements in guinea pigs," *Hear Res.*, vol. 2, no. 3/4, pp. 191–205, Jun. 1980.

[12] P. Magnan *et al.*, "Reverse middle-ear transfer function in the guinea pig measured with cubic difference tones," *Hearing Res.*, vol. 107, no. 1/2, pp. 41–45, 1997.

[13] E. S. Olson, "Observing middle and inner ear mechanics with novel intracochlear pressure sensors," *J. Acoust. Soc. Amer.*, vol. 103, no. 6, pp. 3445–3463, Jun. 1998.

[14] E. S. Olson and S. Borawala, "The design and purpose of an intracochlear pressure sensor," in *Diversity in Auditory Mechanics*, Singapore: World Scientific, 1996, pp. 347–353.

[15] E. S. Olson and H. H. Nakajima, "A family of fiber-optic based pressure sensors for intracochlear measurements," *Photon. Therapeutics Diagnostics Xi*, vol. 9303, 2015, Art. no. 93031O.

[16] M. E. Ravicz *et al.*, "Sound pressure distribution and power flow within the gerbil ear canal from 100 Hz to 80 kHz," *J. Acoust. Soc. Amer.*, vol. 122, no. 4, pp. 2154–2173, Oct. 2007.

[17] S. Puria *et al.*, "Sound-pressure measurements in the cochlear vestibule of human-cadaver ears," *J. Acoust. Soc. Amer.*, vol. 101, no. 5 Pt 1, pp. 2754–2770, May 1997.

[18] J. K. Mattingly *et al.*, "Effects of skin thickness on cochlear input signal using transcutaneous bone conduction implants," *Otol. Neurotol.*, vol. 36, no. 8, pp. 1403–11, Sep. 2015.

[19] H. H. Nakajima *et al.*, "Differential intracochlear sound pressure measurements in normal human temporal bones," *J. Assoc. Res. Otolaryngol.*, vol. 10, no. 1, pp. 23–36, Mar. 2009.

[20] W. P. Eaton and J. H. Smith, "Micromachined pressure sensors: Review and recent developments," *Proc. SPIE*, vol. 3046, pp. 30–41, 1997.

[21] D. T. Martin, "Design, fabrication, and characterization of a MEMS dual-backplate capacitive microphone," Ph.D. dissertation, *Univ. Florida*, Gainesville, FL, USA, 2007.

[22] J. Bryzek, "Impact of MEMS technology on society," *Sensors Actuators A, Phys.*, vol. 56, no. 1–2, pp. 1–9, 8//, 1996.

[23] G. Elko and K. Harney, "The electret meets the micro-electro-mechanical-system," *Acoustics Today*, vol. 5, no. 2, pp. 1–13, 2009.

[24] P. R. Scheeper *et al.*, "A new measurement microphone based on MEMS technology," *J. Microelectromechanical Syst.*, vol. 12, no. 6, pp. 880–891, Dec. 2003.

[25] P. J. Henning and T. Storgaard-Larsen, "MEMS condenser microphone," *J. Acoust. Soc. Amer.*, vol. 108, no. 5, pp. 2495–2495, 2000.

[26] Y. Iguchi *et al.*, "Silicon microphone with wide frequency range and high linearity," *Sensors Actuators A, Phys.*, vol. 135, no. 2, pp. 420–425, Apr. 15 2007.

[27] P. R. Scheeper *et al.*, "Fabrication of silicon condenser microphones using single wafer technology," *J. Microelectromechanical Syst.*, vol. 1, no. 3, pp. 147–154, 1992.

[28] P. R. Scheeper *et al.*, "A review of silicon microphones," *Sensors Actuators A, Phys.*, vol. 44, no. 1, pp. 1–11, Jul. 1994.

[29] Analog Devices Inc. (2013, March) Data Sheet: Specifications ADMP504. [Online]. Available: http://www.analog.com/en/products/obsolete/admp504.html

[30] N. Mohamad *et al.*, "Modelling and optimisation of a spring-supported diaphragm capacitive MEMS microphone," *Engineering*, vol. 2, no. 10, pp. 762–770, 2010.

[31] H. A. C. Tilmans, "Equivalent circuit representation of electromechanical transducers. 1. Lumped-parameter systems (vol 6, pg 157, 1996)," *J. Micromechanics Microeng.*, vol. 6, no. 3, pp. 359–359, Sep. 1996.

[32] A. G. H. Vanderdonk *et al.*, "Modeling of silicon condenser microphones," *Sensors Actuators A, Phys.*, vol. 40, no. 3, pp. 203–216, Mar. 1994.

[33] W. J. Wang *et al.*, "Modeling and characterization of a silicon condenser microphone," *J. Micromechanics Microeng.*, vol. 14, no. 3, pp. 403–409, Mar. 2004.

[34] M. Rossi, "Mechanical and acoustical systems," in *Acoustics and Electroacoustics*. Norwood, MA, USA: Artech House, 1988, pp. 71–374.

[35] M. Füldner, "Modellierung und herstellung kapazitiver mikrofone in BiCMOS-technologie," Ph.D. dissertation, Universität Erlangen-Nürnberg, München, Germany, 2004.

[36] HD MicroSystems (2013, Mar.). Product Bulletin: PI-2600 Series. [Online]. Available: http://www.hdmicrosystems.com/ec/liquid-polyimides-and-pbo-precursors/technical-info.html

[37] J. H. Jerman, "The fabrication and use of micromachined corrugated silicon diaphragms," *Sens. Actuators A, Phys.*, vol. 23, no. 1–3, pp. 988–992, Apr. 1990.

[38] M. Yu and B. Balachandran, "Sensor diaphragm under initial tension: Linear analysis," *Exp. Mechanics*, vol. 45, no. 2, pp. 123–129, Apr. 2005.

[39] F. Schloss and M. Strasberg, "Hydrophone calibration in a vibrating column of liquid," *J. Acoust. Soc. Amer.*, vol. 34, no. 7, pp. 958–959, Jul. 1962.

[40] W. K. Schomburg, *Introduction to Microsystem Design*, Heidelberg, Germany: Springer-Verlag, 2001, pp. 29–50.

[41] R. Gerig *et al.*, "Contribution of the incudo-malleolar joint to middle-ear sound transmission," *Hear Res.*, vol. 327, pp. 218–226, Sep. 2015.

[42] J. H. Sim *et al.*, "Objective assessment of stapedotomy surgery from round window motion measurement," *Ear Hearing*, vol. 33, no. 5, pp. e24–e31, 2012.

[43] *Standard Practice for Describing System Output of Implantable Middle Ear Hearing Devices*, American Soc. Testing and Materials Int., *ASTM F2504 - 05(2014)*, 2014.

Authors' photographs and biographies not available at the time of publication.